

Elucidating Cathode Degradation Mechanisms in $\text{LiNi}_{0.8}\text{Mn}_{0.1}\text{Co}_{0.1}\text{O}_2$ (NMC811)/Graphite Cells Under Fast Charge Rates Using *Operando* Synchrotron Characterization

To cite this article: Calvin D. Quilty *et al* 2022 *J. Electrochem. Soc.* **169** 020545

View the [article online](#) for updates and enhancements.

ECS Toyota Young Investigator Fellowship



For young professionals and scholars pursuing research in batteries, fuel cells and hydrogen, and future sustainable technologies.

At least one \$50,000 fellowship is available annually.
More than \$1.4 million awarded since 2015!



Application deadline: January 31, 2023

Learn more. Apply today!



Elucidating Cathode Degradation Mechanisms in LiNi_{0.8}Mn_{0.1}Co_{0.1}O₂ (NMC811)/Graphite Cells Under Fast Charge Rates Using *Operando* Synchrotron Characterization

Calvin D. Quilty,^{1,2,*} Patrick J. West,^{2,3} Garrett P. Wheeler,^{2,4} Lisa M. Housel,^{2,4} Christopher J. Kern,¹ Killian R. Tallman,^{1,2} Lu Ma,⁵ Steven Ehrlich,⁵ Chernoy Jaye,⁶ Daniel A. Fischer,⁶ Kenneth J. Takeuchi,^{1,2,3,4,**} David C. Bock,^{2,4,z} Amy C. Marschilok,^{1,2,3,4,**,z} and Esther S. Takeuchi^{1,2,3,4,**,z}

¹Department of Chemistry, Stony Brook University, Stony Brook, New York 11794, United States of America

²Institute for Electrochemically Stored Energy, Stony Brook University, Stony Brook, New York 11794, United States of America

³Department of Materials Science and Chemical Engineering, Stony Brook University, Stony Brook, New York 11794, United States of America

⁴Interdisciplinary Science Department, Brookhaven National Laboratory, Upton, New York 11973, United States of America

⁵National Synchrotron Light Source II, Brookhaven National Laboratory, Upton, New York 11973, United States of America

⁶Material Measurement Laboratory, National Institute of Standards and Technology, Gaithersburg, Maryland 20899, United States of America

Li-ion batteries capable of extreme fast charging (XFC) are in demand to facilitate widespread electric vehicle (EV) adoption. While the impact of fast charge on the negative electrode has been studied, degradation of state-of-the-art NMC811 under XFC conditions has not been studied in detail. Herein, cathode degradation is probed in NMC811/graphite batteries by analysis of structural and chemical changes for recovered samples previously cycled under XFC conditions and during typical cycling. NMC surface reconstruction, as determined by soft X-ray absorption, was not detected for recovered electrodes. However, bulk redox activity from X-ray absorption near edge structure measurements showed more change in the oxidation state of Ni and Co under the 1C charge rate compared to the 4C rate consistent with the electrochemistry. Increased unit cell volume contraction under the 1C rate as determined by *operando* X-ray diffraction suggests that higher charge rates may provide a protective effect on the cathode by reducing structural distortion due to less delithiation.

© 2022 The Electrochemical Society ("ECS"). Published on behalf of ECS by IOP Publishing Limited. [DOI: 10.1149/1945-7111/ac51f5]

Manuscript submitted December 12, 2021; revised manuscript received January 6, 2022. Published February 17, 2022. *This paper is part of the JES Focus Issue on Focus Issue In Honor of John Goodenough: A Centenarian Milestone.*

Li ion batteries have become the electrochemical energy storage technology of choice for many portable electronics and transportation applications because of their high energy, high power density, and long lifetime.^{1–3} After invention of framework structures which enabled fast alkali ion transport^{4,5} by John Goodenough in the 1970's, he built upon the concept by establishing that layered lithium oxides LiMO₂ (M = Ni, Co) could be used to reversibly intercalate lithium with voltages near 4.0 V vs Li/Li⁺,^{6,7} approximately twice the voltage of the previously demonstrated Li_xTiS₂ cathode.⁸ These developments paved the way for the first commercialization of a rechargeable Li-ion battery by Sony in 1991 using lithiated metal oxides paired with carbon-based anodes.^{9–11} Since then, batteries using lithium cobalt oxide (LCO) cathode materials have dominated the consumer electronics market due to their high initial Coulombic efficiency and high cycle stability.¹² However, LCO materials cannot be highly delithiated through charge above 4.2 V without incurring side reactions and structural instability,^{12,13} thus limiting their practical capacity. For electric vehicle (EVs) applications, where high energy density is a critical requirement, layered metal oxides based on lithium nickel manganese cobalt oxide (LiNi_xMn_yCo_zO₂, NMC) have been increasingly adopted.^{14–18} In these materials, the inclusion of a high Ni content increases both capacity and operating voltage, Co functions to stabilize the layered structure for enhanced cycle life, and Mn improves the overall thermal and structural stability.^{16,19–21}

While consumer adoption of electric vehicles with Li-ion technology continues to increase, a significant barrier to more widespread implementation is the need for extreme fast charging

capability (XFC, ≤15 min), which would allow EV charging times to be competitive with the refueling times for vehicles powered by conventional internal combustion engines.^{22,23} Recently a major field of study has been devoted to understanding the graphite anode as the limiting electrode under XFC rates where Li plating reactions result in the electrochemical isolation of Li inventory, resulting in loss of capacity with continued cycling.²⁴ However, the degradation mechanisms occurring under fast charge rates at the positive electrode are understudied, especially for state-of-the-art NMC materials with high Ni content.

Under lower charge rates (<1C) causes of capacity fade in NMC materials are known to include (1) large volume changes during cycling resulting in cracking and pulverization of the active material particles^{25–28} and (2) crystal lattice distortion with related cation disordering at particle surfaces resulting in structural transformation of the initial layered rhombohedral (*R3m*) phase to cubic spinel (*Fd3m*) and rocksalt (*Fm3m*) phases, leading to impedance rise accompanied by increased polarization thereby reducing electrochemical reversibility.^{16,17,29–31} Limited studies of NMC positive electrode material degradation have been performed during charging at high rates.^{32–36} Disagreement exists in the literature as to whether particle degradation is more prevalent under higher^{32,33,35} or lower³⁴ rates. It has been shown that Li⁺ loss due to Li-plating can result in higher cathode potentials being accessed, which could result in increased electrolyte oxidation or surface reconstruction, though this has not been verified through experimentation.³⁶ Additionally, capacity fade mechanisms under XFC have not been reported for state-of-the-art Ni-rich LiNi_{0.8}Mn_{0.1}Co_{0.1}O₂ (NMC811) cathodes. With the future of EV batteries moving towards fast charge capability, it is vital to understand the influence of charge rate on positive electrode degradation mechanisms.

The use of synchrotron radiation combined with *operando* methodology provides the opportunity to shed significant insight into the degradation mechanisms occurring at the positive electrode

*Electrochemical Society Student Member.

**Electrochemical Society Member.

***Electrochemical Society Fellow

^zE-mail: dbock@bnl.gov; amy.marschilok@stonybrook.edu; esther.takeuchi@stonybrook.edu

by elucidating the structural and chemical changes that occur during cycling.¹⁵ While the evolution of oxidation state and long-range order in NMC materials have been determined at low rates,^{25,37,38} it is unclear how these fundamental processes are altered under fast charge conditions and if they impact capacity fade. In this work, the *operando* X-ray absorption spectroscopy (XAS) and X-ray diffraction (XRD) measurements on NMC811/graphite batteries under XFC rates are used to quantify unit cell volume and oxidation state evolution during cell cycling. Comparative measurements are also performed under 1C rates, before and after cycling, providing insight into the effect of rate on positive electrode aging.

Experimental Methods

Cell fabrication.—NMC811 cathodes were prepared from a slurry of 90% NMC811, 5% carbon, and 5% polyvinylidene fluoride (PVDF) in N-methylpyrrolidone (NMP) that was tape-cast on aluminum foil (1.6 mAh cm⁻², 60 μm thick, 8 +/- 4 μm particle size). Graphite anodes were prepared from a slurry of 90% graphite, 3% carbon, and 7% PVDF in NMP that was tape-cast on copper foil (1.6 mAh cm⁻², 50 μm thick, 12 +/- 5 μm particle size). These electrodes were fabricated into pouch cells with polyethylene separator and a 1 mol L⁻¹ LiPF₆ 3:7 (by volume) ethylene carbonate: dimethyl carbonate (EC:DMC) electrolyte. The cell stacks were vacuum sealed in aluminized plastic housings.

Electrochemical testing.—Cells were cycled on a Biologic VSP multichannel potentiostat and MACCOR multichannel testing system at 30 °C. All cells underwent three formation cycles at C/10 (1C = 190 mA g⁻¹) from 3 V to 4.3 V. Cells were then cycled 150 times from 3 V to 4.3 V at a 1C discharge rate and a charge rate of either 1C or 4C. *Operando* XRD and XAS measurements were conducted at the Quick X-ray Absorption and Scattering (QAS, 7-BM) beamline at the National Synchrotron Light Source II at Brookhaven National Laboratory. XRD and XAS scans each took approximately sixty seconds. Cells were cycled once according to the cycling conditions noted above while XRD and XAS measurements were collected. Additionally, one cell was cycled twice at QAS after formation; the cell was cycled from 3.0 V to 4.3 V at a discharge rate of 1C and a charge rate of 6C for the first charge and 8C for the second charge. XRD measurements were collected with an amorphous Si detector with a CsI scintillator; the wavelength was calibrated to 0.6204 Å with an SRM660 LaB₆ standard. All patterns were analyzed by Rietveld refinements using the GSAS-II software.³⁹ XAS data was collected at the Ni and Co K-edges, 8333 eV and 7709 eV, respectively. Duplicate XAS scans were collected and all data processing was done in Athena.⁴⁰ Linear combination fitting in Athena was performed on all X-ray absorption

near edge structure (XANES) spectra using a fit range of (-30 to 30) eV in a μ(E) fitting space. Three electrode cells were fabricated using a cell configuration with a working electrode area of 7.1 cm². The reference electrode in the three electrode cells was lithium metal. The 3-electrode cells underwent formation cycling in a 2-electrode configuration followed by a charging step to 50% state of charge (SOC). Charge pulse testing was performed at 4C and 6C rates starting at 50% SOC for each pulse train.

Soft X-ray absorption spectroscopy (sXAS) characterization.—Positive electrodes were harvested in the discharged state from graphite/NMC811 cells post formation or post cycling under 1C or 6C charge rates and 1C discharge rate. Cathodes were rinsed, dried, and kept under inert atmosphere prior to analysis. sXAS measurements were collected at beamline 7-ID-1 at the National Synchrotron Light Source II at Brookhaven National Laboratory. The Ni L-edge was measured in the range (840 to 880) eV under 10⁻⁹ Torr vacuum. Measurements were collected in three detection modes: partial electron yield (PEY), total electron yield (TEY) and fluorescence yield (FY). Data processing was done using the software program Athena and Origin.⁴⁰

Results and Discussion

The effect of charge rate and cycle number on the structural and chemical evolution of Ni-rich LiNi_{0.8}Mn_{0.1}Co_{0.1}O₂ (NMC811) was investigated through the study of cells after formation and after 150 cycles at 1C discharge and charge at either 1C or 4C to 4.3 V prior to synchrotron measurement (Fig. 1). Charging at the slower 1C rate resulted in 7% higher delivered capacity initially, while after 150 cycles the delivered capacities were 158 mAh g⁻¹ and 147 mAh g⁻¹ for cells cycled using the 1C and 4C charge rates, respectively.

Operando XRD and XAS measurements were collected on four cells where both cycling condition (post formation vs. post 150 cycles) and charge rate (1C vs. 4C) were considered (Table I). The electrochemical behavior of the cells during the *operando* XRD and XAS measurements are shown in Fig. 2. The observed electrochemistry was consistent with the formation cycling data, showing that 1C charging results in higher delivered capacity both before and after 150 cycles, but the amount of capacity fade was similar independent of charging rate, at ca. 11%. Excellent temporal resolution for the XRD and XAS measurements was achieved even under the 4C charging condition due to the short (≈ 60 s) data collection times enabled by the synchrotron.

Unit cell evolution in NMC materials during charging occurs in two phases. In the first phase occurring during moderate delithiation (≈ 0.67 electron equivalents), the *a* lattice parameter contracts and the *c* parameter expands leading to a small volume contraction; in the

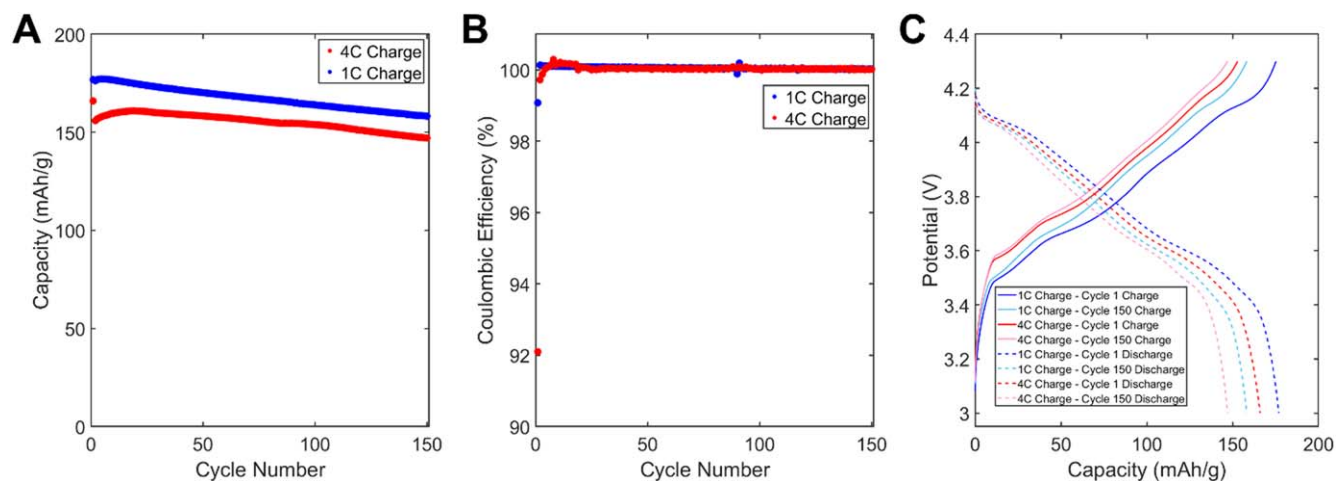
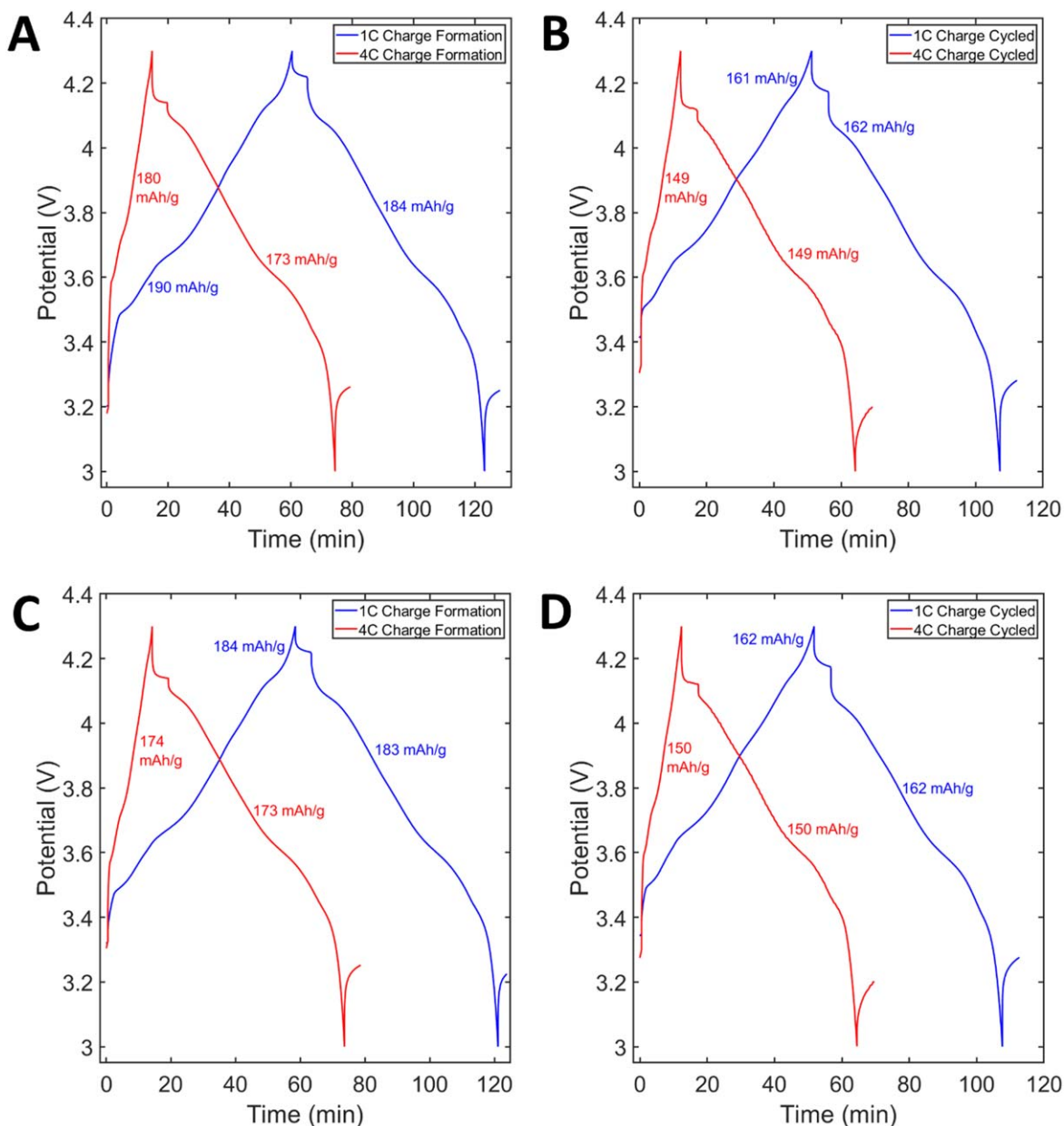


Figure 1. (A) Discharge capacity and (B) Coulombic efficiency vs. cycle number for graphite/NMC811 cells cycled 150 times between 3.0 V and 4.3 V at 1C or 4C charge rates, with 1C discharge. (C) Voltage curves for the first and 150th cycles.

Table I. Formation and beamline cycling conditions for graphite/NMC811 cells measured using *operando* XRD/XAS.

Formation cycling condition	<i>Operando</i> beamline cycling condition	Cell designation
Formation cycling (3 to 4.3) V, C/10, 4 cycles)	1C charge, 1C discharge	1C Charge Formation
Formation cycling (3 to 4.3) V, C/10, 4 cycles)	4C charge, 1C discharge	4C Charge Formation
Formation + 150 cycles, 1C charge, 1C discharge	1C charge, 1C discharge	1C Charge Cycled
Formation + 150 cycles, 4C charge, 1C discharge	4C charge, 1C discharge	4C Charge Cycled

**Figure 2.** Galvanostatic cycling during (A), (B) *operando* XRD and (C), (D) *operando* XAS measurements of the (A), (C) formation cells and (B), (D) cycled cells.

second phase which occurs during deep delithiation (>0.67 electron equivalents), there is a sharp drop in the c parameter and a significant contraction in the unit cell volume.^{25,37} These changes were tracked by the *operando* X-ray diffraction measurements (Fig. 3). For the cells charged at 1C, more significant shift to higher angle of several of the diffraction peaks was observed, indicative of greater contraction in the NMC unit cell during charging as compared to cells that were charged at 4C. For example, the peak shown in the insets (Fig. 3), initially

shifts to lower angle during charge and then at higher states of charge shifts to a significantly higher angle. This suggests an expansion along the c axis followed by a substantial contraction that is more pronounced for 1C charging. This greater contraction is consistent with the higher delivered capacities at the 1C charging rate, 190 mAh g^{-1} vs 180 mAh g^{-1} .

To gain quantitative insight into the observed unit cell evolutions, all XRD patterns were fitted using Rietveld refinement. The key

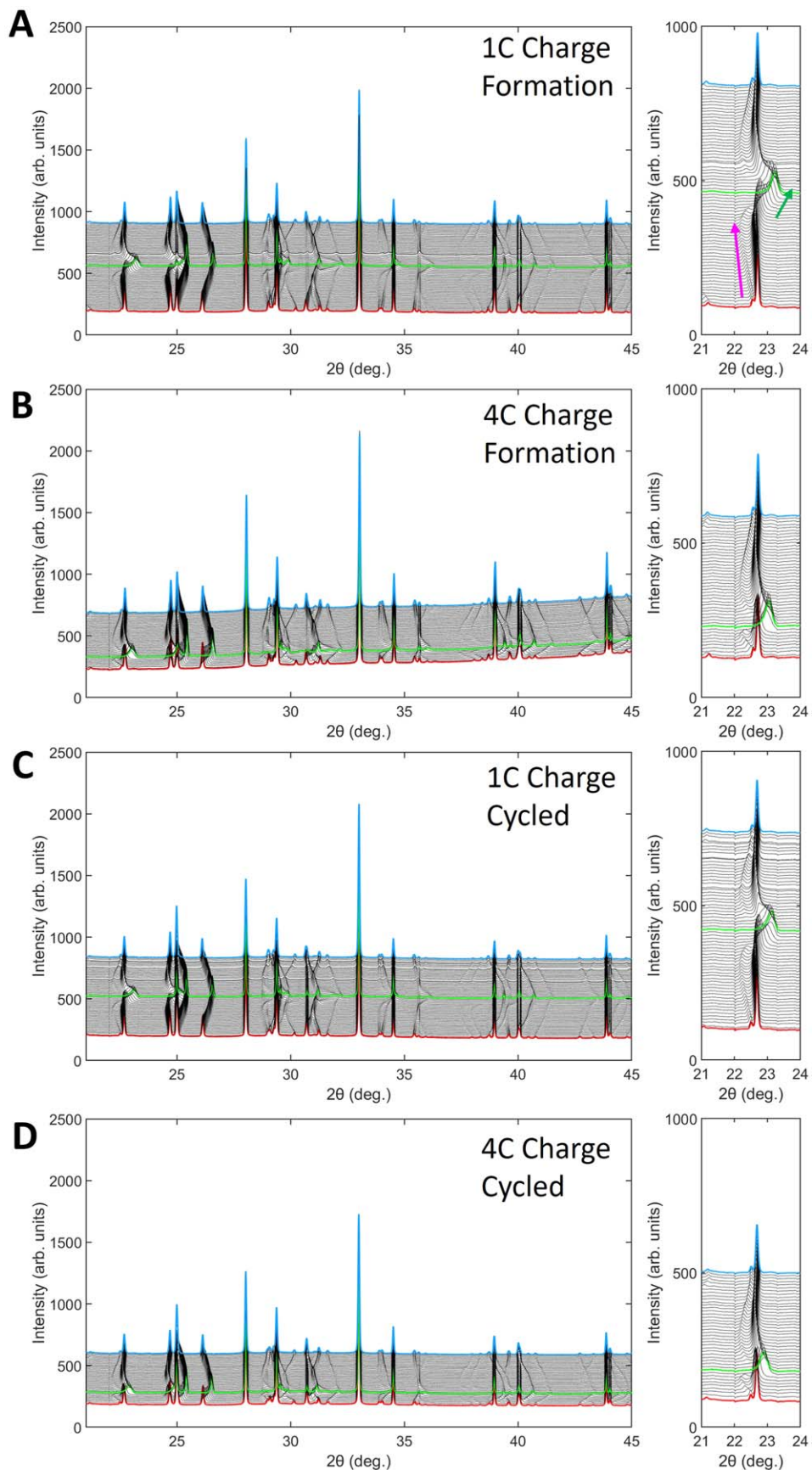


Figure 3. Operando XRD of the (A) 1C Charge Formation cell, (B) 4C Charge Formation cell, (C) 1C Charge Cycling cell, and (D) 4C Charge Cycling cell. Red is the initial state, green is the charged state, and blue is the discharged state. The intense peaks at 28 and 33° are associated with the copper current collector. The magenta arrow in (A) indicates the initial c axis expansion, while the green arrow indicates the subsequent, sharp c axis contraction.

results of these refinements are shown in Fig. 4. In all four cells during charging, the a lattice parameter contracts from 2.86 Å to 2.82 Å, the c parameter expands from 14.28 Å to 14.48 Å and then contracts sharply to ≈ 14 Å, where the volume contracts first slowly and then more quickly at deeper levels of delithiation. These changes were reversed upon discharging (lithiation) indicating good reversibility in the system. Notably, greater volume changes were observed for the 1C charging cells: 5.8% for 1C Charge Formation and 5.1% for 1C Charge Cycled, compared with 4.6% and 3.5% observed for the 4C Charge Formation and 4C Cycled cells respectively. Greater volume changes during cycling have been linked with detrimental impact including pulverization of the micrometer-scale NMC particles, causing capacity fade through loss of electrical contact, rising impedance, and additional side reactions on the new surfaces generated.^{17,25,37} The increased volume contraction for cells cycled under 1C charge rate may account for the initially surprising similarity in capacity retention for the two conditions. 4C charging likely leads to increased loss of capacity through lithium plating at the negative electrode,^{41,42} however this loss may be offset by the better structural integrity of the positive electrode at the lower level of delithiation demonstrated at the high current charge conditions.

Operando XANES spectra were collected on all four cell types to probe the differences in redox behavior of the metal centers as a function of charge rate and cycle number (Fig. 5). A significant shift towards higher energy in the nickel K-edge was observed during charge for all four cells tested, and the edge positions returned to their initial position during discharge. Similarly, a shift towards higher energy at the Co K-edge upon charge occurred that reversed during discharge, indicating reversible redox activity at the Ni and Co metal centers.

Linear combination fitting was performed to determine quantitatively the redox evolution during the *operando* measurements, Fig. 6. The oxidation state of manganese was confirmed to be 4+. This was accomplished by fitting the Mn K-edge of an NMC811 standard with Mn K-edge spectra from Mn_2O_3 and MnO_2 standards. The LCF results show that the NMC811 Mn K-edge can be best fit as the summation of 100% MnO_2 (Mn^{4+}) and 0% Mn_2O_3 (Mn^{3+}) suggesting that Mn in NMC811 is Mn^{4+} . Cobalt K-edge *operando* data was fit using two standards: a LiCoO_2 standard and an electrochemically delithiated $\text{Li}_{0.389}\text{CoO}_2$ standard ($\text{Co}^{3.611+}$). The charged standard data was obtained by charging LiCoO_2 where the stoichiometry was determined from the electrochemical data. Nickel oxidation state was calculated based on electroneutrality, where Mn and Co oxidation state were determined using linear combination fitting, and lithium content was calculated based on the electrochemistry. Consistent with the qualitative observations, significant reversible Ni redox ($\approx 3.1+$ to $3.9+$) and Co redox ($\approx 3+$ to $3.6+$) occurred during cycling. The 1C Charge Formation cell exhibited the highest levels of Ni and Co redox activity, with changes in oxidation state of 0.8 and 0.6 respectively, consistent with the higher delivered capacity for this cell. The 4C Charge Formation cell showed only slightly lower redox activity, 0.7 for Ni and 0.5 for Co. Notably, these results indicate that electrochemical activity of Ni vs Co was not significantly different under 1C vs. 4C charge rates. For cells tested after 150x cycles, the total redox activity decreased, with changes in oxidation state of 0.7 and 0.5 of Ni and Co redox for the 1C Charge Cycled cell and only 0.6 and 0.5 for the 4C Charge Cycled cell.

To test the oxidation state evolution at even higher XFC rates, *operando* XAS data were collected on a cell, post-formation, that

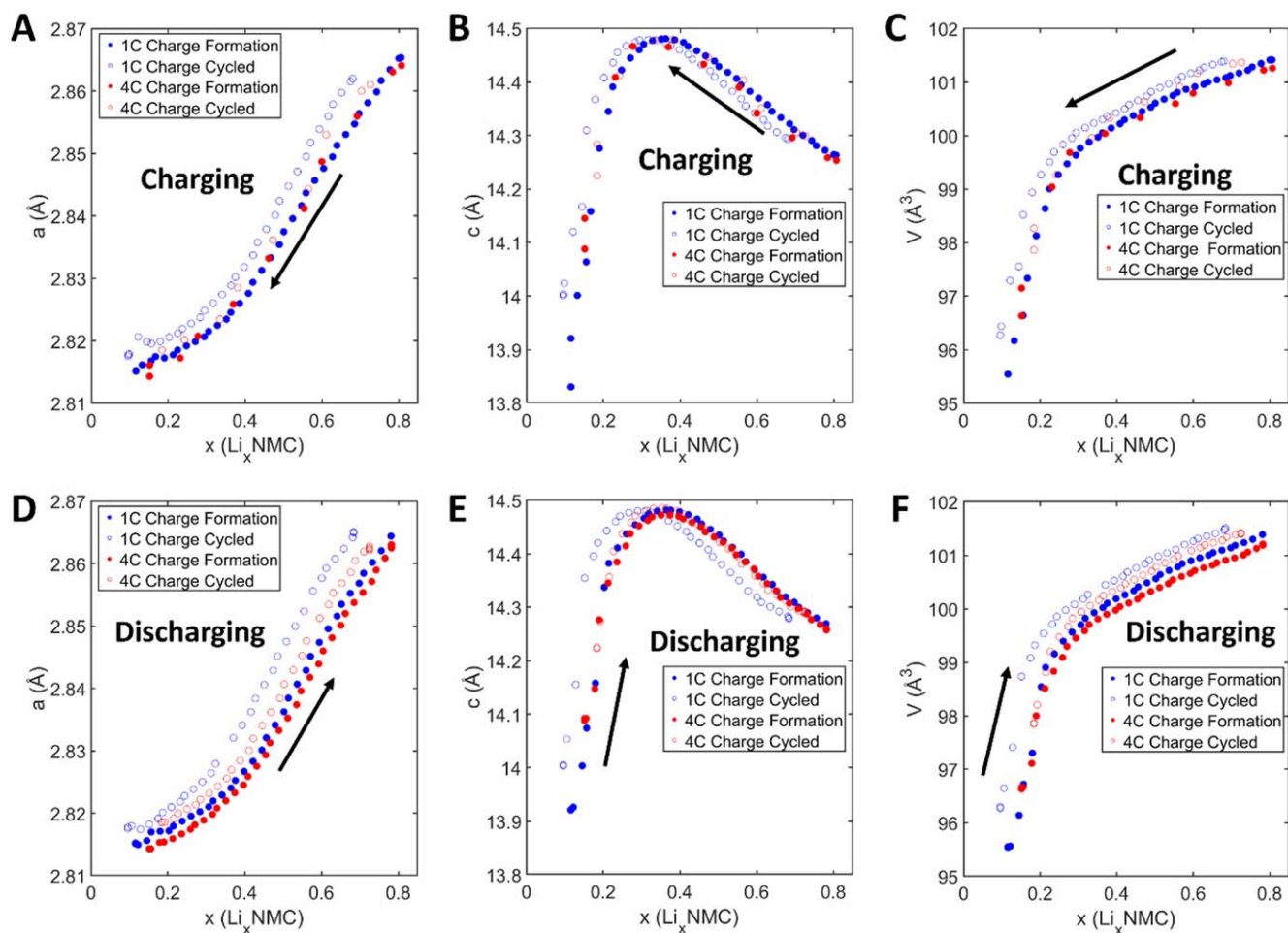


Figure 4. (A), (D) a lattice parameters, (B), (E) c lattice parameters, and (C), (F) unit cell volumes obtained by Rietveld refinement of the *operando* XRD data.

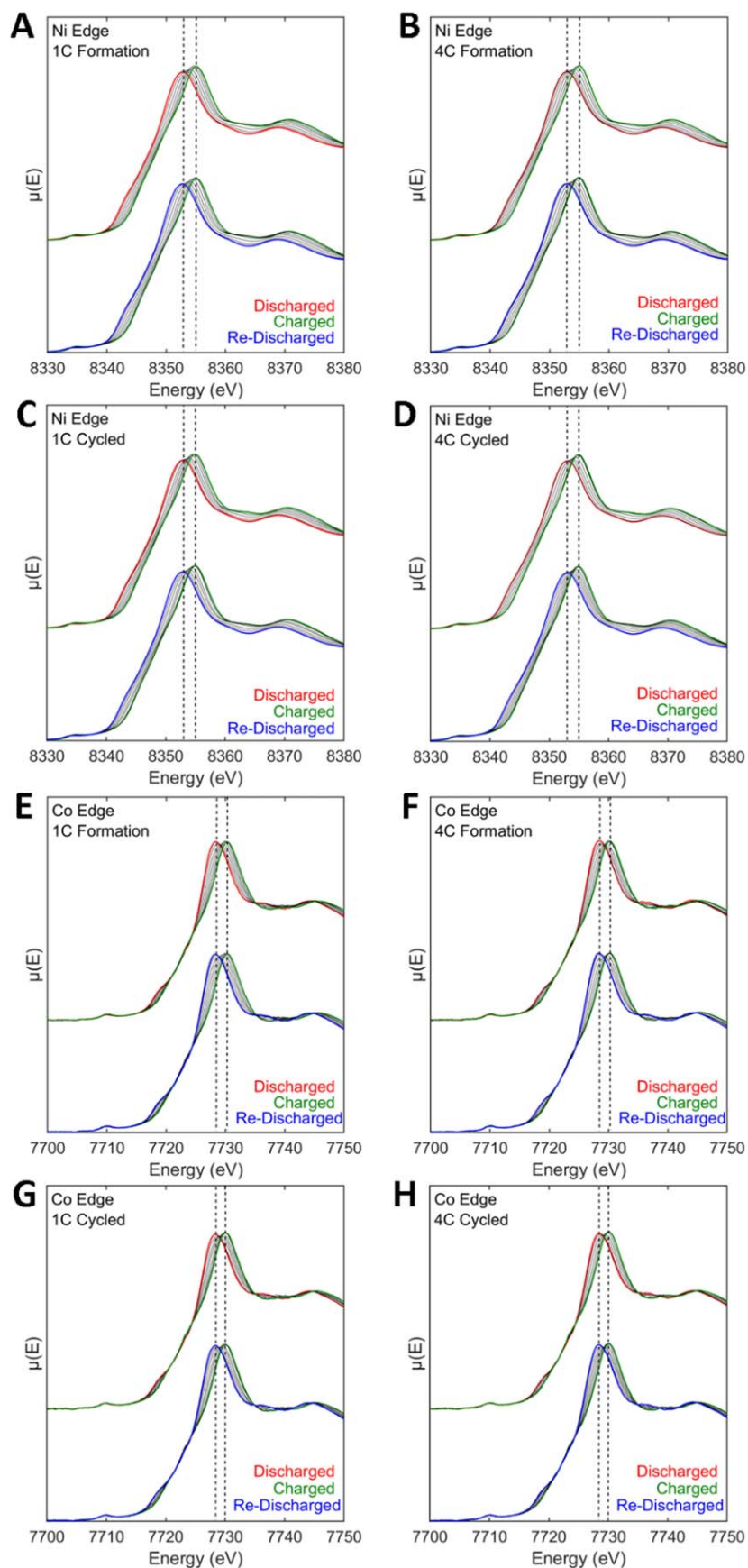


Figure 5. Operando XANES spectra collected on the Ni and Co edges of the 1C Charge Formation cell (A), (E), the 4C Charge Formation cell (B), (F), the 1C Charge Cycled cell (C), (G), and the 4C Charge Cycled cell (D), (H).

was charged under 6C and then under 8C rate with a 1C discharge rate (Figs. 7, 8). The cell delivered a capacity of 163 mAh g^{-1} under 6C charge and 142 mAh g^{-1} under 8C charge with moderate

decreases in delivered capacity following the 6C and 8C charge steps (Table II). The XANES data showed a slight decrease in nickel and cobalt oxidation in the charged state as rate increased from 1C to 8C,

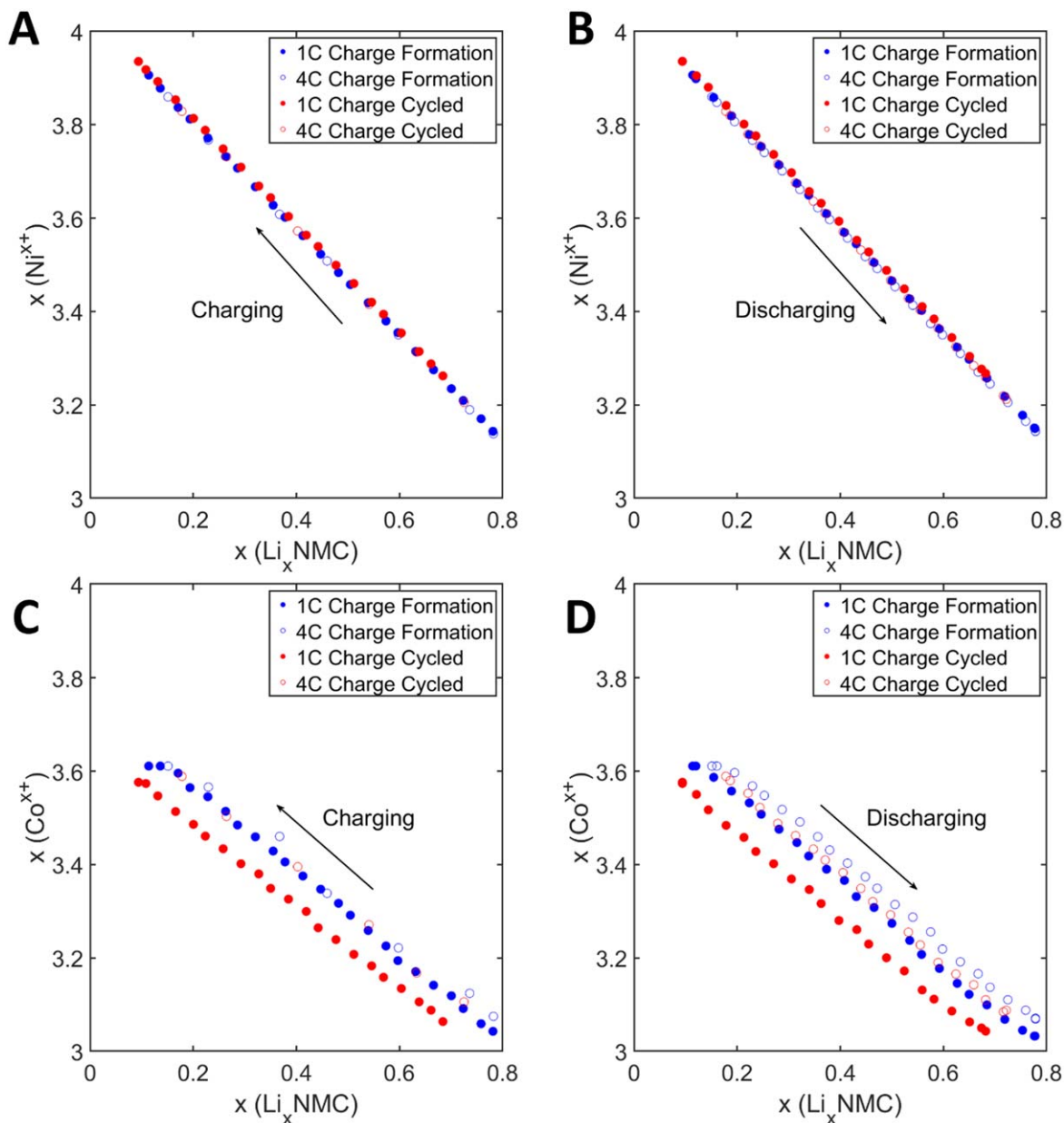


Figure 6. Oxidation states of nickel and cobalt as determined by linear combination fitting of the XANES data. (A) The oxidation state of nickel during charging, (B) the oxidation state of nickel during discharging, (C) the oxidation state of cobalt during charging, and (D) the oxidation state of cobalt during discharging.

where charging at 1C resulted in Ni and Co oxidation states of 3.91+ and 3.61+, while 8C led to 3.74+ and 3.40+, respectively.

To probe the contributions of the negative and positive electrodes under fast charge rates, 3-electrode cells were intermittently charged under 4C and 6C rates starting at 50% SOC. For each rate, 4 charge segments were performed, where each segment was 30 s followed by a 10-min open circuit rest period. Between charge segments, the cells were charged at C/10 rate for one hour, where high rate intervals were collected at 50%, 60%, 70%, and 80% SOC. Representative voltage responses for the cell, positive, and negative electrodes are shown in Fig. 9, and quantified DC resistances are shown in Fig. 10. At high rates, significant polarization of the positive electrode occurs, reaching 4.3 V at $\approx 80\%$ state of charge under the 4C rate and by 60% state of charge under the 6C rate. The positive electrode contribution to cell

resistance is significant ranging between 50% and 80% depending on state of charge. It is also noted that negative electrode voltage polarization was below 0 V vs. Li/Li⁺ at 60% SOC, indicating opportunity for Li plating.

sXAS measurements were collected on positive electrodes in the discharged state post formation and post cycling with 1C and 6C charge rates, 1C discharge rate, to probe the possible presence of reduced surface oxidation states associated with surface reconstruction phases, that have been implicated in impedance buildup and reduced electrochemical reversibility.^{43,44} Measurements were collected in three detection modes: partial electron yield (PEY), total electron yield (TEY) and fluorescence yield (FY) with depth sensitivities of *ca.* (1 to 2) nm, 5 nm, and (50 to 100) nm, respectively.^{15,45} These measurements probe dipole allowed 2p-3d excitations (L_{2,3}-edges) for the transition metals, where the edges are

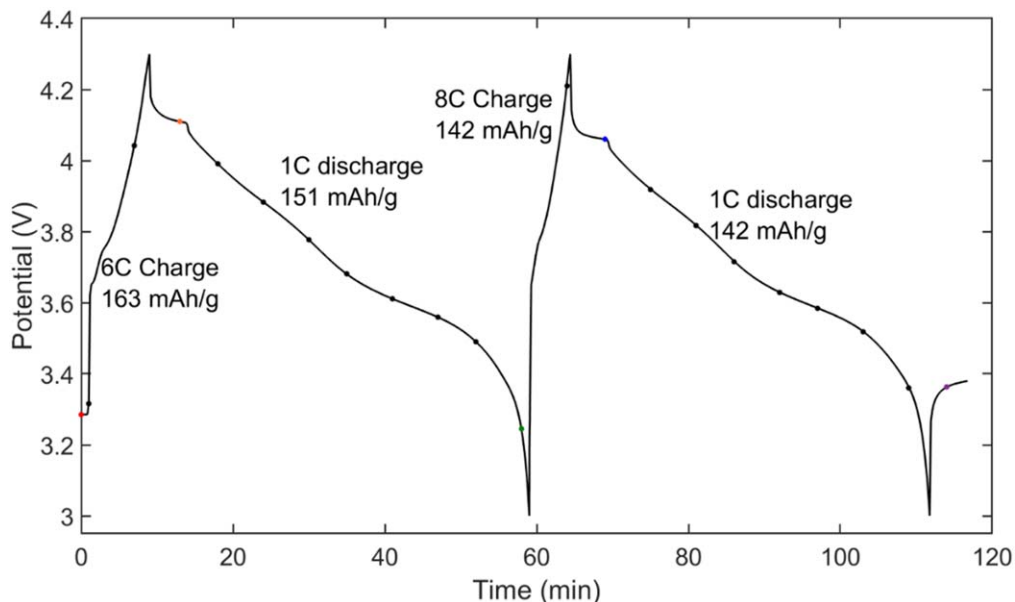


Figure 7. Galvanostatic cycling during *operando* XAS measurements of the formation cell charged to 6C and 8C with 1C discharges. Black dots indicate time points where XAS data was collected.

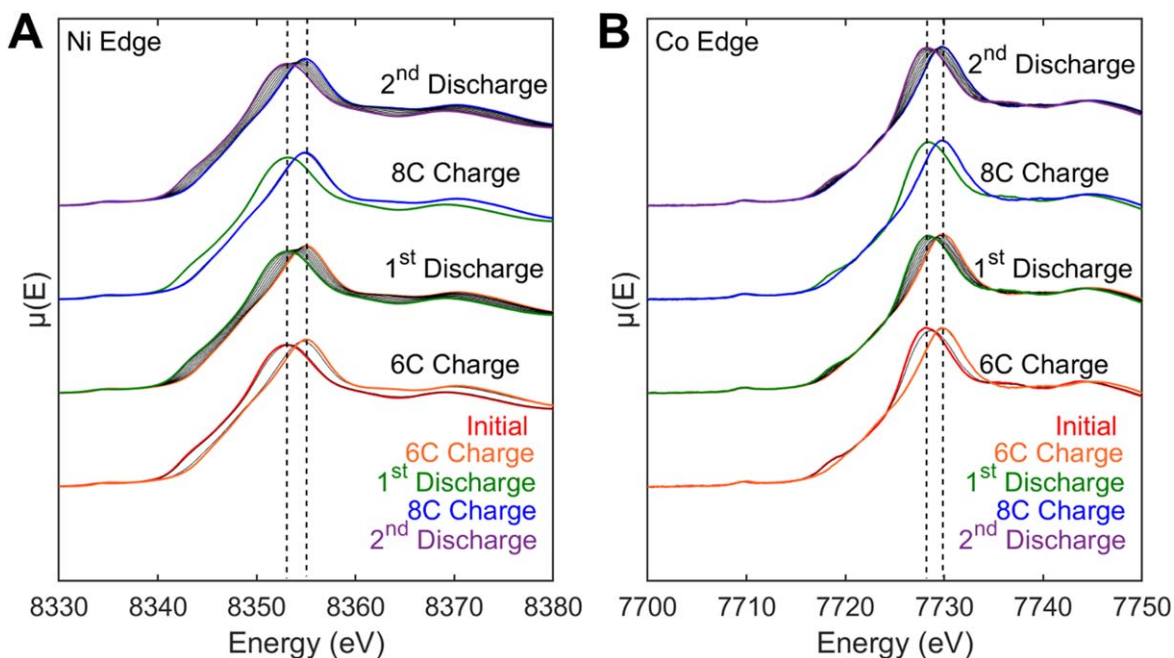


Figure 8. *Operando* XANES spectra collected on the (A) Ni and (B) Co edges of the formation cell in the discharged state (red), after charging at 6C (orange), after discharging at 1C (green), after charging at 8C (blue), and after discharging again at 1C (purple).

sensitive to the occupancy of the 3d orbitals.⁴⁶ Ni L-edge measurements are presented in Fig. 11 for PEY, TEY, and FY detection modes. Closer inspection of the Ni L₃-edge reveals that the multiplet is split into two peaks. Changes in the intensity ratio of the Ni L₃ High to L₃ low peaks, denoted as γ , are an indicator for Ni oxidation state, where γ increases as Ni is oxidized.^{15,47} The γ values for the samples as well as Ni²⁺ and Ni³⁺ standards are presented in Fig. 11D. The electrode cycled using the 1C charge rate had a similar γ value as the formation cycled electrode, indicating similar oxidation state. However, there was a significant increase in γ value for the electrode cycled using the 6C charge rate, indicative of increased Ni oxidation state in the discharged state. These results suggest that (1) surface reconstruction is not a significant degradation mechanism during cycling under high charge rate as this would be indicated by a

Table II. Charge capacities and Ni and Co oxidation states in the charged state for four charge rates.

Charge Rate	Charge Capacity (mAh/g)	x (Ni ^{x+})	x (Co ^{x+})
1C	190	3.91	3.61
4C	180	3.86	3.61
6C	163	3.78	3.43
8C	142	3.74	3.40

reduced surface charge which was not observed, and (2) instead, loss of active lithium due to irreversible Li plating at the negative electrode is an important cause of capacity fade.

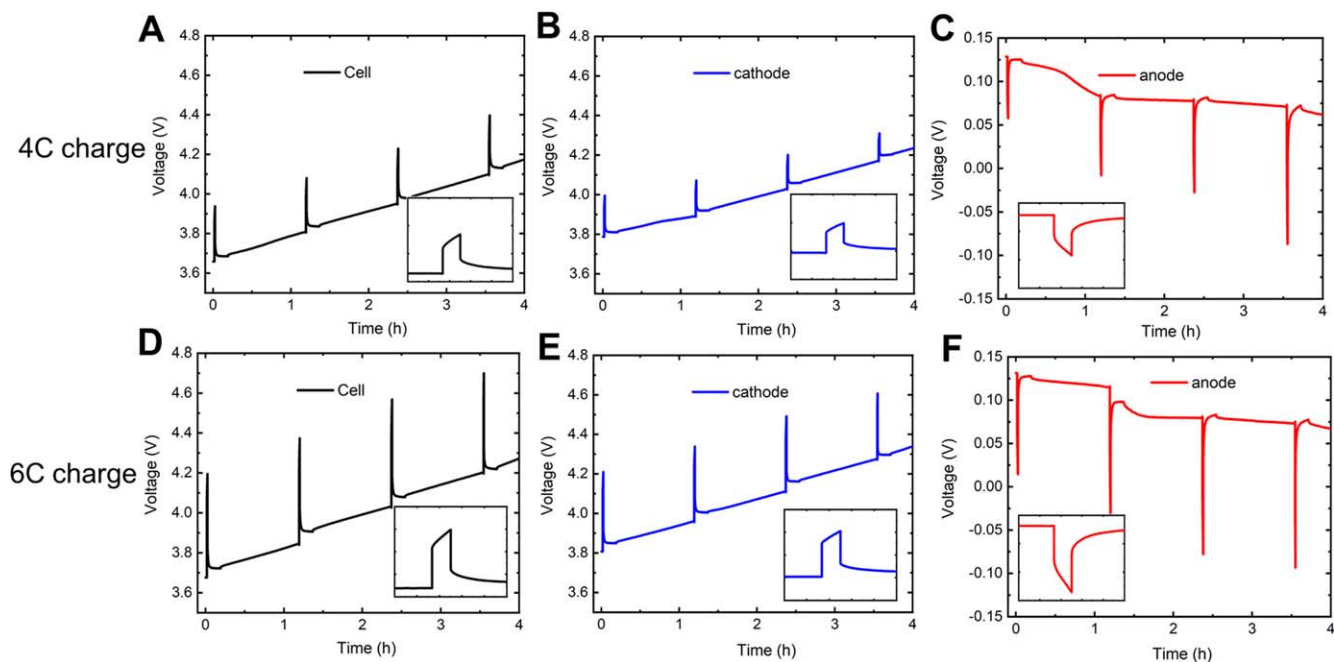


Figure 9. Intermittent charge testing under (A)–(C) 4C and (D)–(F) 6C rates using 3-electrode cells with NMC cathode, graphite anode, and Li reference. Representative voltage response is shown for (A), (D) the cell, (B), (E) the working electrode, and (C), (F) the counter electrode. The charge protocol consisted of four 30 s steps at the XFC rate, with C/10 galvanostatic charge for 1 h in between steps. Insets in (A)–(C) show the representative voltage profiles during the first step at each rate.

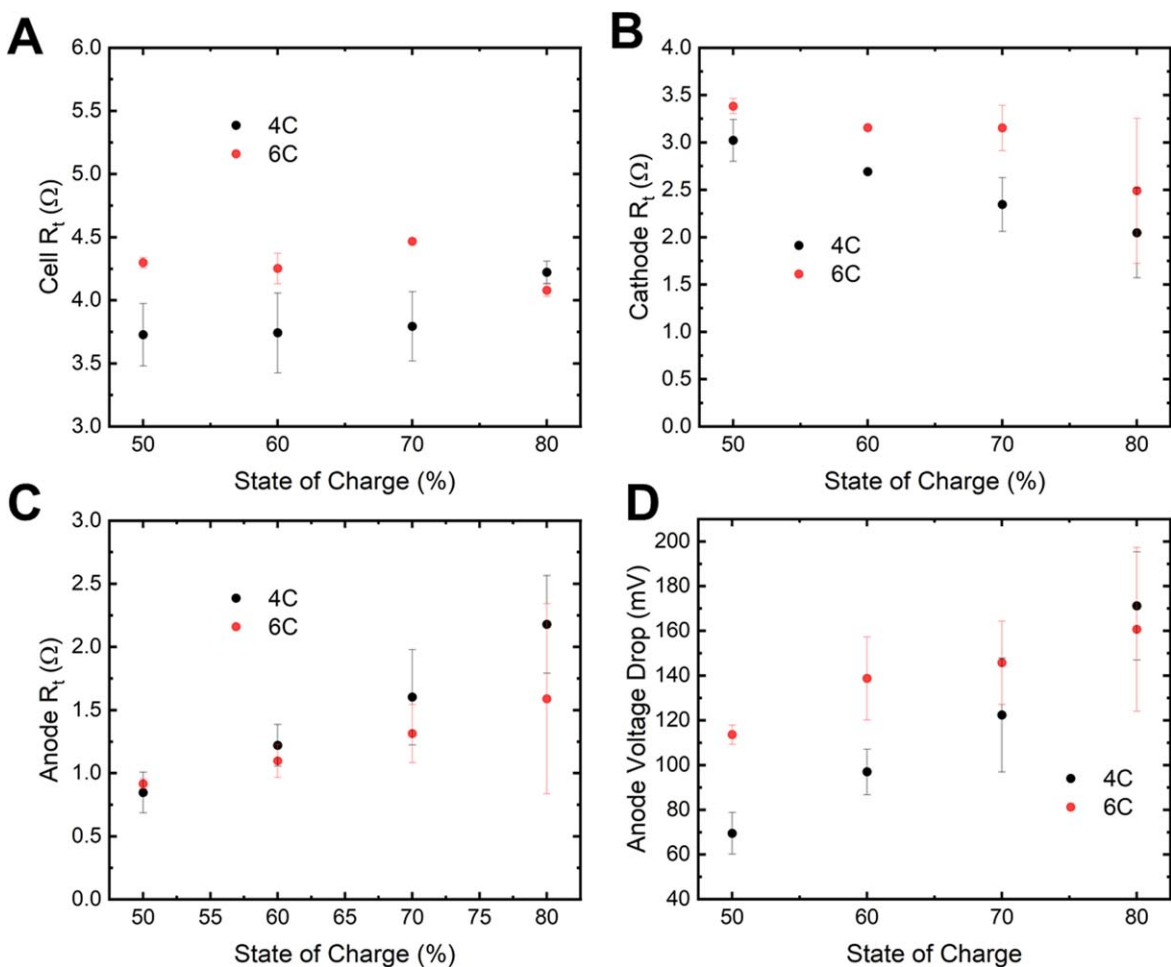


Figure 10. Total DC resistances of (A) the cell, (B) cathode, and (C) anode as well as (D) anode voltage drop during 4C and 6C pulses using 3-electrode cells ($n = 3$). Error bars represent one standard deviation.

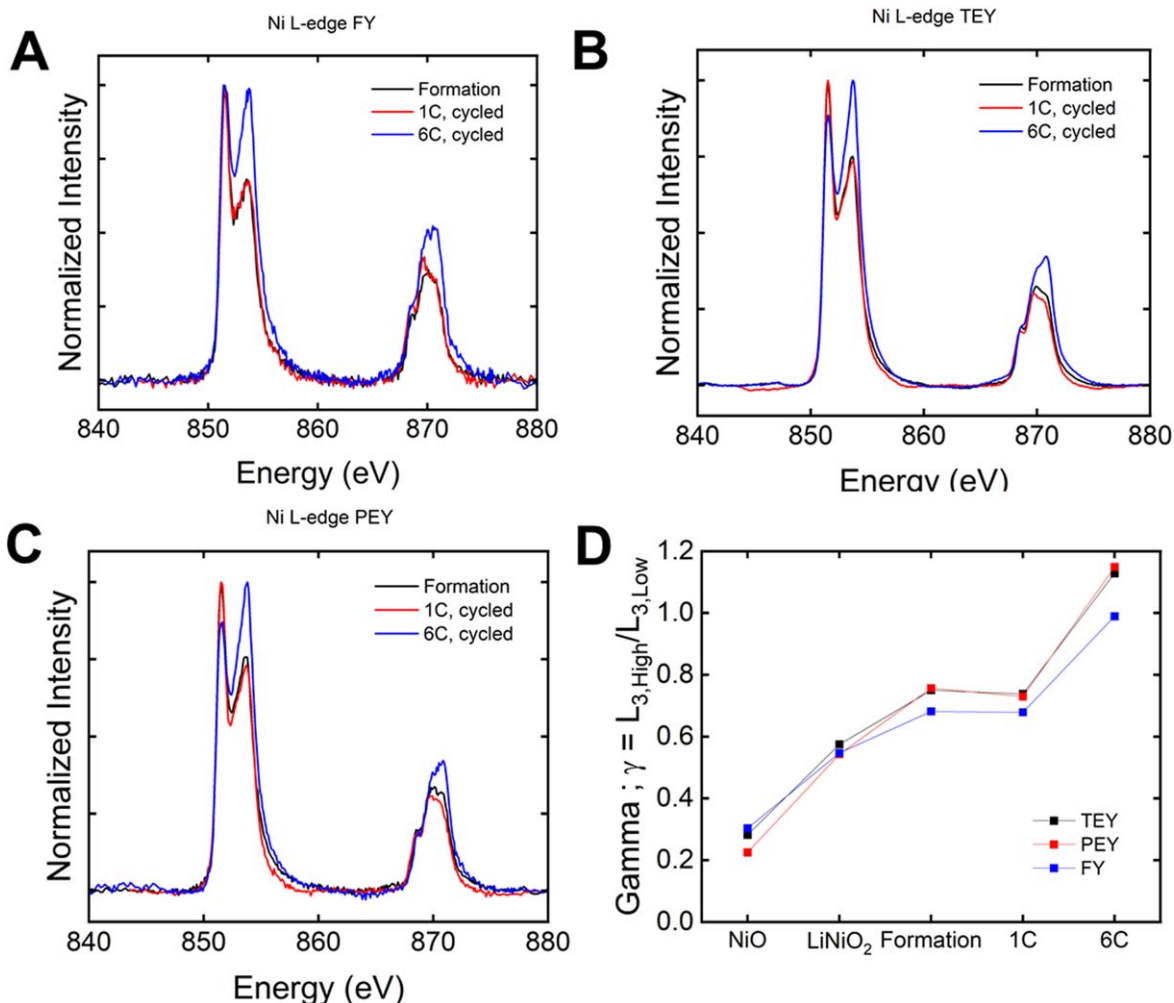


Figure 11. Soft XAS Ni L-edge spectra for an NMC811 electrode after formation cycling, an electrode after cycling under 1C rate charge rate, and an electrode after cycling under 6C charge rate using different detection modes: (A) fluorescence yield, (B) total electron yield, (C) partial electron yield. (D) The ratio between the peak intensities of the Ni $L_{3, \text{High}}$ and $L_{3, \text{Low}}$ peaks of the Ni L-edge, γ , for the three electrodes as well as NiO and LiNiO₂ standards.

Conclusions

The results presented include *operando* XRD and XAS experiments on graphite/NMC811 batteries while cycling under a fast charge protocol. The XAS results reveal that the electrochemical activity of Ni in NMC811 is different under 1C vs. 4C charge rates. Three-electrode cell measurements under XFC conditions indicate polarization of the anode below 0 V, while *ex situ* sXAS measurements of the positive electrode show no evidence of surface reconstruction as a capacity fade mechanism. The most notable difference was an increased volume contraction for cells cycled under 1C rate as determined by X-ray diffraction consistent with the higher reversible capacity. This may result in reduced structural integrity of the positive electrode over extended cycling due to higher levels of delithiation compared to higher rates of charge. Thus, the fast charge rates may have a protective effect on the positive electrode by preventing high levels of structural distortion that occur during deep delithiation.

Acknowledgments

X-ray absorption spectroscopy analysis was sponsored by the DEVCOM Army Research Laboratory (ARL) and was funded under Cooperative Agreement (CA) Number W911NF-20-2-0284. The views and conclusions contained in this document are those of the

authors and should not be interpreted as representing the official policies, either expressed or implied, of the DEVCOM Army Research Laboratory or the U.S. Government. The U.S. Government is authorized to reproduce and distribute reprints for Government purposes notwithstanding any copyright notation hereon. Three-electrode cell studies were supported by the U. S. Department of Energy Office of Energy Efficiency and Renewable Energy under the Advanced Battery Materials Research program, award DE-EE0007785. Methodology for *operando* data collection was supported as part of the Center for Mesoscale Transport Properties, funded by the U.S. Department of Energy, Office of Science, Basic Energy Sciences, under Award #DE-SC0012673 for financial support. X-ray diffraction analysis was supported by Mercedes-Benz Research and Development North America (MBRDNA). This research used resources of beamline 7-BM Quick X-ray Absorption and Scattering (QAS) and beamline 7-ID-1 Spectroscopy Soft and Tender (SST-1) of the National Synchrotron Light Source II, a U.S. Department of Energy (DOE), Office of Science User Facility operated by the DOE Office of Science by Brookhaven National Laboratory under Contract No. DE-SC0012704. E.S.T. acknowledges support as the William and Jane Knapp Chair in Energy and the Environment. Identification of commercial names in this paper is for illustrative purpose and not intended to imply recommendation or endorsement by the National Institute of Standards and Technology.

Author Contributions

The manuscript was written through contributions of all authors. All authors have given approval to the final version of the manuscript.

ORCID

Patrick J. West  <https://orcid.org/0000-0002-8717-9538>
 Kenneth J. Takeuchi  <https://orcid.org/0000-0002-9345-6503>
 Amy C. Marschilok  <https://orcid.org/0000-0001-9174-0474>
 Esther S. Takeuchi  <https://orcid.org/0000-0001-8518-1047>

References

- M. S. Whittingham, "Lithium batteries and cathode materials." *Chem. Rev.*, **104**, 4271 (2004).
- M. M. Thackeray, C. Wolverton, and E. D. Isaacs, "Electrical energy storage for transportation—approaching the limits of, and going beyond, lithium-ion batteries." *Energy Environ. Sci.*, **5**, 7854 (2012).
- L. Lu, X. Han, J. Li, J. Hua, and M. Ouyang, "A review on the key issues for lithium-ion battery management in electric vehicles." *J. Power Sources*, **226**, 272 (2013).
- J. B. Goodenough, H. Y. P. Hong, and J. A. Kafalas, "Fast Na⁺-ion transport in skeleton structures." *Mater. Res. Bull.*, **11**, 203 (1976).
- J. B. Goodenough, "Cathode materials: A personal perspective." *J. Power Sources*, **174**, 996 (2007).
- K. Mizushima, P. C. Jones, P. J. Wiseman, and J. B. Goodenough, "Li_xCoO₂ (0 < x < 1): A new cathode material for batteries of high energy density." *Mater. Res. Bull.*, **15**, 783 (1980).
- J. Goodenough, K. Mizushima, and T. Takeda, "Solid-solution oxides for storage-battery electrodes." *Jpn. J. Appl. Phys.*, **19**, 305 (1980).
- M. S. Whittingham, "Electrical energy storage and intercalation chemistry." *Science*, **192**, 1126 (1976).
- A. Yoshino and K. Sanechika, "Secondary Battery." *Japanese Patent*, No. 2668678 (1986).
- A. Yoshino, K. Sanechika, and T. Nakajima, "Secondary Battery." *Japanese Patent*, No. 1989293 (1985).
- A. Yoshino and K. Sanechika, "Nonaqueous secondary battery." *Japanese Patent*, No. 2128922 (1984).
- L. Wang, B. Chen, J. Ma, G. Cui, and L. Chen, "Reviving lithium cobalt oxide-based lithium secondary batteries-toward a higher energy density." *Chem. Soc. Rev.*, **47**, 6505 (2018).
- C. J. Patridge, C. T. Love, K. E. Swider-Lyons, M. E. Twigg, and D. E. Ramaker, "In-situ X-ray absorption spectroscopy analysis of capacity fade in nanoscale-LiCoO₂." *J. Solid State Chem.*, **203**, 134 (2013).
- F. Schipper, E. M. Erickson, C. Erk, J.-Y. Shin, F. F. Chesneau, and D. Aurbach, "Review—recent advances and remaining challenges for lithium ion battery cathodes: I. Nickel-Rich, LiNi_xCoyMnzO₂." *J. Electrochem. Soc.*, **164**, A6220 (2017).
- C. Tian, D. Nordlund, H. L. Xin, Y. Xu, Y. Liu, D. Sokaras, F. Lin, and M. M. Doeff, "Depth-dependent redox behavior of LiNi_{0.6}Mn_{0.2}Co_{0.2}O₂." *J. Electrochem. Soc.*, **165**, A696 (2018).
- C. Tian, F. Lin, and M. M. Doeff, "Electrochemical characteristics of layered transition metal oxide cathode materials for lithium ion batteries: surface, bulk behavior, and thermal properties." *Acc. Chem. Res.*, **51**, 89 (2018).
- M. D. Radin, S. Hy, M. Sina, C. Fang, H. Liu, J. Vinckeviciute, M. Zhang, M. S. Whittingham, Y. S. Meng, and A. Van der Ven, "Narrowing the gap between theoretical and practical capacities in Li-Ion layered oxide cathode materials." *Adv. Energy Mater.*, **7**, 20 (2017).
- D. Andre, S.-J. Kim, P. Lamp, S. F. Lux, F. Maglia, O. Paschos, and B. Stiaszny, "Future generations of cathode materials: an automotive industry perspective." *J. Mater. Chem. A*, **3**, 6709 (2015).
- A. Manthiram, J. C. Knight, S.-T. Myung, S.-M. Oh, and Y.-K. Sun, "Nickel-rich and lithium-rich layered oxide cathodes: progress and perspectives." *Adv. Energy Mater.*, **6**, 1501010-n/a (2016).
- S.-K. Jung, H. Gwon, J. Hong, K.-Y. Park, D.-H. Seo, H. Kim, J. Hyun, W. Yang, and K. Kang, "Understanding the degradation mechanisms of LiNi_{0.5}Co_{0.2}Mn_{0.3}O₂ cathode material in lithium ion batteries." *Adv. Energy Mater.*, **4**, 1300787 (2014).
- S.-M. Bak, E. Hu, Y. Zhou, X. Yu, S. D. Senanayake, S.-J. Cho, K.-B. Kim, K. Y. Chung, X.-Q. Yang, and K.-W. Nam, "Structural changes and thermal stability of charged LiNi_{0.5}Mn_{0.3}Co_{0.2}O₂ cathode materials studied by combined in situ time-resolved XRD and Mass spectroscopy." *ACS Appl. Mater. Interfaces*, **6**, 22594 (2014).
- S. Ahmed, I. Bloom, A. N. Jansen, T. Tanim, E. J. Dufek, A. Pesaran, A. Burnham, R. B. Carlson, F. Dias, K. Hardy, M. Keyser, C. Kreuzer, A. Markel, A. Meintz, C. Michelbacher, M. Mohanpurkar, P. A. Nelson, D. C. Robertson, and J. Zhang, "Enabling fast charging—A battery technology gap assessment." *J. Power Sources*, **367**, 250 (2017).
- W. Yourey, Y. Fu, N. Li, V. Battaglia, and W. Tong, "Determining accelerated charging procedure from half cell characterization." *J. Electrochem. Soc.*, **166**, A1432 (2019).
- W. Cai, Y.-X. Yao, G.-L. Zhu, C. Yan, L.-L. Jiang, C. He, J.-Q. Huang, and Q. Zhang, "A review on energy chemistry of fast-charging anodes." *Chem. Soc. Rev.*, **49**, 3806 (2020).
- A. O. Kondrakov, A. Schmidt, J. Xu, H. Gesswein, R. Moenig, P. Hartmann, H. Sommer, T. Brezesinski, and J. Janek, "Anisotropic lattice strain and mechanical degradation of high- and Low-Nickel NCM cathode materials for Li-Ion batteries." *J. Phys. Chem. C*, **121**, 3286 (2017).
- H. Gao, J. Cai, G.-L. Xu, L. Li, Y. Ren, X. Meng, K. Amine, and Z. Chen, "Surface Modification for suppressing interfacial parasitic reactions of a nickel-rich lithium-ion cathode." *Chem. Mater.*, **31**, 2723 (2019).
- K. Ishidzu, Y. Oka, and T. Nakamura, "Lattice volume change during charge/discharge reaction and cycle performance of Li[Ni_xCo_yMn_zO₂]." *Solid State Ionics*, **288**, 176 (2016).
- E.-J. Lee, Z. Chen, H.-J. Noh, S. C. Nam, S. Kang, D. H. Kim, K. Amine, and Y.-K. Sun, "Development of microstrain in aged lithium transition metal oxides." *Nano Lett.*, **14**, 4873 (2014).
- C. Xu, K. Marker, J. Lee, A. Mahadevegowda, P. J. Reeves, S. J. Day, M. F. Groh, S. P. Emge, C. Ducati, B. L. Mehdi, C. C. Tang, and C. P. Grey, "Bulk fatigue induced by surface reconstruction in layered Ni-rich cathodes for Li-ion batteries." *Nat. Mater.*, **20**, 84 (2021).
- S. Li, Z. Jiang, J. Han, Z. Xu, C. Wang, H. Huang, C. Yu, S.-J. Lee, P. Pianetta, H. Ohldag, J. Qiu, J.-S. Lee, F. Lin, K. Zhao, and Y. Liu, "Mutual modulation between surface chemistry and bulk microstructure within secondary particles of nickel-rich layered oxides." *Nat. Commun.*, **11**, 4433 (2020).
- F. Lin, I. M. Markus, D. Nordlund, T.-C. Weng, M. D. Asta, H. L. Xin, and M. M. Doeff, "Surface reconstruction and chemical evolution of stoichiometric layered cathode materials for lithium-ion batteries." *Nat. Commun.*, **5**, 3529 (2014).
- S. Xia, L. Mu, Z. Xu, J. Wang, C. Wei, L. Liu, P. Pianetta, K. Zhao, X. Yu, F. Lin, and Y. Liu, "Chemomechanical interplay of layered cathode materials undergoing fast charging in lithium batteries." *Nano Energy*, **53**, 753 (2018).
- S.-B. Son, D. Robertson, Z. Yang, Y. Tsai, S. Lopykinski, and I. Bloom, "Fast charge-driven Li plating on anode and structural degradation of cathode." *J. Electrochem. Soc.*, **167**, 140506 (2020).
- R. Xu, L. S. de Vasconcelos, J. Shi, J. Li, and K. Zhao, "Disintegration of meatball electrodes for LiNi_xMn_yCo_zO₂ cathode materials." *Exp. Mech.*, **58**, 549 (2018).
- T. R. Tanim, E. J. Dufek, M. Evans, C. Dickerson, A. N. Jansen, B. J. Polzin, A. R. Dunlop, S. E. Trask, R. Jackman, and I. Bloom, "Extreme fast charge challenges for lithium-ion battery: variability and positive electrode issues." *J. Electrochem. Soc.*, **166**, A1926 (2019).
- A. Raj, M.-T. F. Rodrigues, and D. P. Abraham, "Rate-dependent aging resulting from fast charging of Li-Ion cells." *J. Electrochem. Soc.*, **167**, 120517 (2020).
- C. D. Quilty, D. C. Bock, S. Yan, K. J. Takeuchi, E. S. Takeuchi, and A. C. Marschilok, "Probing Sources of capacity fade in LiNi_{0.6}Mn_{0.2}Co_{0.2}O₂ (NMC622): an operando XRD study of Li/NMC622 batteries during extended cycling." *J. Phys. Chem. C*, **124**, 8119 (2020).
- K. R. Tallman, G. P. Wheeler, C. J. Kern, E. Stavitski, X. Tong, K. J. Takeuchi, A. C. Marschilok, D. C. Bock, and E. S. Takeuchi, "Nickel-rich nickel manganese cobalt (NMC622) cathode lithiation mechanism and extended cycling effects using operando X-ray absorption spectroscopy." *The Journal of Physical Chemistry C*, **125**, 58 (2021).
- B. H. Toby and R. B. Von Dreele, "GSAS-II: the genesis of a modern open-source all purpose crystallography software package." *J. Appl. Crystallogr.*, **46**, 544 (2013).
- B. Ravel and M. Newville, "ATHENA, ARTEMIS, HEPHAESTUS: data analysis for X-ray absorption spectroscopy using IFFEFIT." *J. Synchrotron Radiat.*, **12**, 537 (2005).
- T. Waldmann, B.-I. Hogg, and M. Wohlfahrt-Mehrens, "Li plating as unwanted side reaction in commercial Li-ion cells—A review." *J. Power Sources*, **384**, 107 (2018).
- P. R. Chinnam, A. M. Colclasure, B.-R. Chen, T. R. Tanim, E. J. Dufek, K. Smith, M. C. Evans, A. R. Dunlop, S. E. Trask, B. J. Polzin, and A. N. Jansen, "Fast-charging aging considerations: incorporation and alignment of cell design and material degradation pathways." *ACS Appl. Energy Mater.*, **4**, 9133 (2021).
- B. Gilbert, B. H. Frazer, A. Belz, P. G. Conrad, K. H. Nealon, D. Haskel, J. C. Lang, G. Srajer, and G. De Stasio, "Multiple scattering calculations of bonding and X-ray absorption spectroscopy of manganese oxides." *The Journal of Physical Chemistry A*, **107**, 2839 (2003).
- S. Hy, W.-N. Su, J.-M. Chen, and B.-J. Hwang, "Soft X-ray Absorption Spectroscopic and Raman Studies on Li_{1.2}Ni_{0.2}Mn_{0.6}O₂ for Lithium-Ion Batteries." *The Journal of Physical Chemistry C*, **116**, 25242 (2012).
- J. W. Smith and R. J. Saykally, "Soft X-ray absorption spectroscopy of liquids and solutions." *Chem. Rev.*, **117**, 13909 (2017).
- F. M. F. de Groot, J. C. Fuggle, B. T. Thole, and G. A. Sawatzky, "2p X-ray absorption of 3d transition-metal compounds: An atomic multiplet description including the crystal field." *Physical Review B*, **42**, 5459 (1990).
- F. Lin, I. M. Markus, D. Nordlund, T.-C. Weng, M. D. Asta, H. L. Xin, and M. M. Doeff, "Surface reconstruction and chemical evolution of stoichiometric layered cathode materials for lithium-ion batteries." *Nat. Commun.*, **5**, 3529 (2014).